# In-focus monochromator: theory and experiment of a new grazing incidence mounting

Michael C. Hettrick

Applied Optics Vol. 29, Issue 31, pp. 4531-4535 (1990)

http://dx.doi.org/10.1364/AO.29.004531

9. A. B. C. Walker, T. W. Barbee, R. B. Hoover, and J. F. Lindblom, "Soft X-Ray Images of the Solar Corona with a Normal Incidence Cassegrain Multilayer Telescope," Science **241**, 1781–1787 (1989).
10. L. Golub *et al.*, "Sub-arcsecond Observations of the Solar X-ray Corona," Nature London **344**, 842–844 (1990).
11. J. C. Rife, W. R. Hunter, T. W. Barbee, Jr., and R. G. Cruddace, "Multilayer-Coated Blazed Grating Performance in the Soft X-Ray Region," Appl. Opt. **28**, 2984–2986 (1989).
12. T. W. Barbee, "Combined Microstructure X-Ray Optics," Rev. Sci. Instrum. **260**, 1588 (1989).
13. J. C. Rife, T. W. Barbee, W. R. Hunter, and R. G. Cruddace, "Performance of a Tungsten/Carbon Multilayer-Coated Blazed Grating from 150 to 1700 eV," Phys. Scr. **41**, 418 (1990).
14. R. G. Cruddace, T. W. Barbee, J. C. Rife, and W. R. Hunter, "Measurements of the Normal-Incidence X-Ray Reflectance of a Molybdenum-Silicon Multilayer Deposited on a 200 l/mm Grating," Phys. Scr. **41**, 396 (1990).
15. J. V. Bixler, T. W. Barbee, and D. D. Dietrich, "Performance of Multilayer Coated Gratings in the Extreme Ultraviolet," Proc. Soc. Photo-Opt. Instrum. Eng. **1160**, 648–654 (1989).
16. W. M. Neupert, G. L. Epstein, R. J. Thomas, and U. Feldman, "A Solar Ultraviolet Telescope and Spectrograph for Shuttle/Spacelab," Space Sci. Rev. **29**, 425–429 (1981).
17. A. P. Bradford, G. Hass, J. F. Osantowski and A. R. Toft, "Preparation of Mirror Coatings for the Vacuum Ultraviolet in the 2-m Evaporator," Appl. Opt. **8**, 1183 (1969).
18. J. F. Osantowski, "Reflectance and Optical Constants for Cer-Vit from 250 to 1050 Å," J. Opt. Soc. Am. **64**, 834 (1974).
19. B. E. Patchett *et al.*, "CDS—The Coronal Diagnostic Spectrometer," The SOHO Mission—Scientific and Technical Aspects of the Instruments, ESA SP-1104 (1989), pp. 39–42.

## In-focus monochromator: theory and experiment of a new grazing incidence mounting

Michael C. Hettrick

Hettrick Scientific, Inc., P.O. Box 8046, Kensington, California 94707.
Received 6 June 1990.
Sponsored by William R. Hunter, Springfield, Virginia.
0003-6935/90/314531-05$02.00/0.


*A varied-space grating mounted to both rotate and translate constitutes a practical single element fixed slit monochromator which is in focus at all wavelengths.* Keywords: *Monochromators, diffraction gratings, grazing incidence, x-ray optics.*

No self-focusing reflection grating has hitherto delivered spectral images which remain in focus to first power in the aperture over a continuum of wavelengths diffracted between fixed entrance and exit slits. Rowland circle designs[1,2] require movable slits, whereas plane grating monochromators employ auxiliary mirrors[3–7] which lower the throughput and introduce figuring and alignment errors. Fixed slit designs where a concave grating simply rotates to select the wavelength are practically in focus at near normal incidence[8] but suffer from severe defocusing at grazing incidence.[3,9]

These limitations are overcome with a new optical design, whose essential features are shown in Fig. 1. A reflection grating consists of grooves whose spacings vary continuously across its ruled width. To select the desired transmitted wavelength, the grating is rotated about an axis fixed in space, while simultaneously being translated along its surface in the direction of its ruled width. Due to the varied spacing, the translation provides a new set of effective grating parameters where the principal ray strikes the grating surface. The freedom to choose the amount of translation permits each wavelength to be brought into an exact focus (to first power) at the fixed exit slit. The novelty of this scheme may be appreciated from the fact that such a translation would have no effect on the properties of a conventional (equally spaced) grating.

This degree of freedom inherent in varied-space gratings has previously been left unexploited, except for theoretical designs requiring a prohibitively large exponential variation in spacing.[10] The combined rotation and translation of a (varied-space) grating is a new mounting; hence the grating itself must be derived from a new focusing condition rather than as an improvement in any classical grating.

The extent to which the optical aberrations are controlled is best analyzed if the local groove density of the grating is expanded as a power series in the grating aperture:

$$1/\sigma = 1/\sigma_0 + N_2 w + N_3 w^2 + N_4 w^3 + \ldots, \quad (1)$$

where $\sigma_0$ is the nominal groove spacing at the grating center ($w = 0$); $N_2$, $N_3$, $N_4$, etc. are varied-space constants; and $w$ is the ruled width coordinate as projected on the plane tangent to the grating at its center.

The wavelength diffracted through an infinitesimally narrow exit slit by the grooves in the vicinity of coordinate $w$ will differ from that diffracted by the grating center by an amount

$$\Delta\lambda = (\sigma_0/m)(F_2/w + \tfrac{3}{2}F_3 w^2 + 2F_4 w^3 + \ldots), \quad (2)$$

where $m$ is the spectral order, and $F_2$, $F_3$, $F_4$, etc. are the Fermat aberration coefficients. The image is considered to be in-focus at the exit slit if the first power aberration $F_2 = 0$. Finite $F_3$ values result in a comatic image whose profile is asymmetrical, while the third power $F_4$ term is spherical aberration, present even along the classical Rowland circle. To minimize the total amount of translation required over a finite spectral region, we first consider rotation only of the grating to select two wavelengths, $\lambda_1$ and $\lambda_2$, and adjust the design parameters to minimize the aberrations there. Even with the constraint of fixed slits, $F_2$ and $F_3$ may be made to vanish at both wavelengths if the grating is concave ($0 < R < \infty$), resulting in the following focusing condition:

$$1/r = (\sqrt{b^2 - 4ac} - b)/(2aR), \quad (3)$$

$$1/r' = \delta/r - \epsilon/R, \quad (4)$$

$$N_2 = (T_1 + T_1')/(m\lambda_1), \quad (5)$$

$$N_3 = \tfrac{3}{2}[T_1(\sin\alpha_1)/r - T_1'(\sin\beta_1)/r']/(m\lambda_1), \quad (6)$$

where $T = (\cos^2\alpha)/r - (\cos\alpha)/R$, $T' = (\cos^2\beta)/r' - (\cos\beta)/R$,

$$a = \gamma \sin\alpha_1 \cos^2\alpha_1 - \sin\alpha_2 \cos^2\alpha_2 - \gamma\delta^2 \sin\beta_1 \cos^2\beta_1 + \delta^2 \sin\beta_2 \cos^2\beta_2, \quad (7)$$

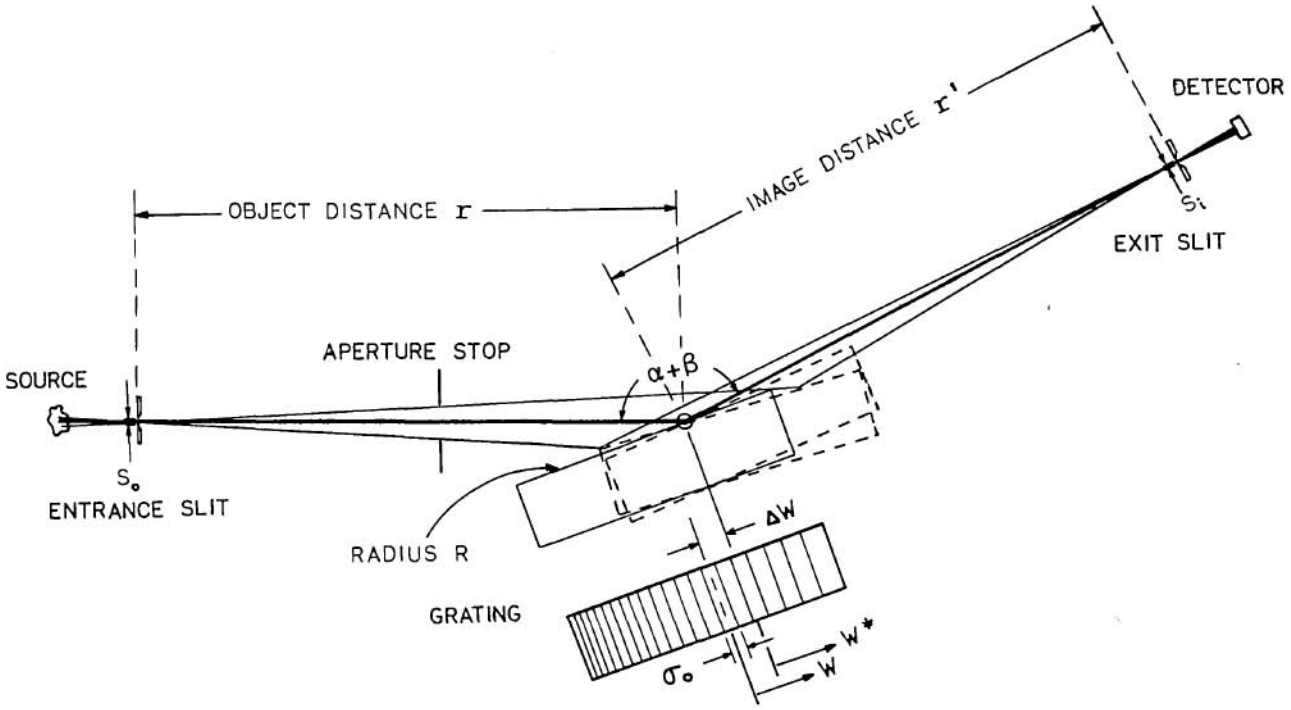


Fig. 1. Basic optical configuration of the monochromator. The upper portion shows a section taken across the meridional plane of the grating. A reflection grating rotates about a fixed axis (open circle) while translating along its surface in the direction of its varied groove spacing. The fixed principal ray is indicated by dark lines. The grating position is drawn solid for a typical wavelength and dashed for two extreme wavelengths at opposite ends of the spectral range of a concave grating embodiment. The bottom portion is a top view of the grating surface, schematically showing the varied spacing.

$$b = -\gamma \sin\alpha_1 \cos\alpha_1 + \sin\alpha_2 \cos\alpha_2 + 2\gamma\delta\epsilon \sin\beta_1 \cos^2\beta_1 - 2\delta\epsilon \sin\beta_2 \cos^2\beta_2 + \gamma\delta \sin\beta_1 \cos\beta_1 - \delta \sin\beta_2 \cos\beta_2, \quad (8)$$

$$c = -\gamma\epsilon^2 \sin\beta_1 \cos^2\beta_1 + \epsilon^2 \sin\beta_2 \cos^2\beta_2 - \gamma\epsilon \sin\beta_1 \cos\beta_1 + \epsilon \sin\beta_2 \cos\beta_2, \quad (9)$$

$$\delta = (\gamma \cos^2\alpha_1 - \cos^2\alpha_2)/(\cos^2\beta_2 - \gamma \cos^2\beta_1), \quad (10)$$

$$\epsilon = [\gamma(\cos\alpha_1 + \cos\beta_1) - (\cos\alpha_2 + \cos\beta_2)]/(\cos^2\beta_2 - \gamma \cos^2\beta_1), \quad (11)$$

$$\gamma = \lambda_2/\lambda_1, \quad (12)$$

where $R$ is the grating radius of curvature, $r$ is the object distance, $r'$ is the image distance, and $\alpha$ and $\beta$ are the angles of incidence and diffraction, respectively, relative to the grating surface normal. All values are measured from the fixed axis of rotation, which for simplicity is assumed to intersect the grating at its center.

For example, a design tailored to extreme UV wavelengths may have as input parameters $\sigma_0 = 1/1500$ mm, $R = 10$ m, constant deviation $\alpha + \beta = 164°$, $m = +1$, $\lambda_1 = 100$ Å, and $\lambda_2 = 200$ Å. Equations (3)–(12) then provide the design parameters $r = 1011.488$ mm, $r' = 964.542$ mm, $N_2 = -1.63766$ mm$^{-2}$, and $N_3 = +0.00267255$ mm$^{-3}$. These differ substantially from those of a conventional concave grating monochromator.

Using the above parameters and a 50-mm illuminated aperture, curves 200, 202, and 204 of Fig. 2 are the individual optical aberrations of Eq. (2) with only grating rotation to select the wavelength. As constrained above, the resolution is extremely high in the immediate vicinity of the two wavelengths, $\lambda_1$ and $\lambda_2$. However, it degrades rapidly elsewhere, dominated by a large amount of defocusing (curve 200). The maximum defocus of 0.5 Å is nearly as poor as the 0.7 Å resulting from an equally spaced grating design[9] of the same aperture, system length, angular deviation, and groove density (curves 100, 102, and 104).

The key to removal of defocusing aberrations, and hence the usefulness of the present grating design, is a translation of the grating at all wavelengths other than $\lambda_1$ and $\lambda_2$. Considering simple linear translation in the direction of the tangent plane at the grating center results in the following substitutions:

$$w \rightarrow w^* = w - \Delta w, \quad (13)$$

$$1/\sigma_0 \rightarrow 1/\sigma_0^* = 1/\sigma_0(1 - \tfrac{1}{2}\phi^2) + N_2\Delta w(1 - \tfrac{2}{3}\phi^2) + N_3\Delta w^2 + N_4\Delta w^3, \quad (14)$$

$$N_2 \rightarrow N_2^* = -\phi/(R\sigma_0) + N_2(1 - 2\phi^2) + 2N_3\Delta w + 3N_4\Delta w^2, \quad (15)$$

$$N_3 \rightarrow N_3^* = -\phi^2/(4R^2\sigma_0) - \tfrac{3}{2}N_2(1 + \tfrac{2}{9}\phi^2)\phi/R + N_3(1 + \tfrac{1}{2}\phi^2) + 3N_4(1 + \tfrac{1}{6}\phi^2)\Delta w, \quad (16)$$

$$N_4 \rightarrow N_4^* = -\tfrac{2}{3}\phi/R^3\sigma_0) - \tfrac{4}{3}N_2(\phi/R)^2 + \tfrac{4}{3}N_3\phi/R + N_4(1 + 2\phi^2), \quad (17)$$

where

$$\phi = \arcsin(\Delta w/R), \quad (18)$$

$\Delta w$ being the amount of translation in the direction of the decreasing ruled width. The fixed principal ray now strikes

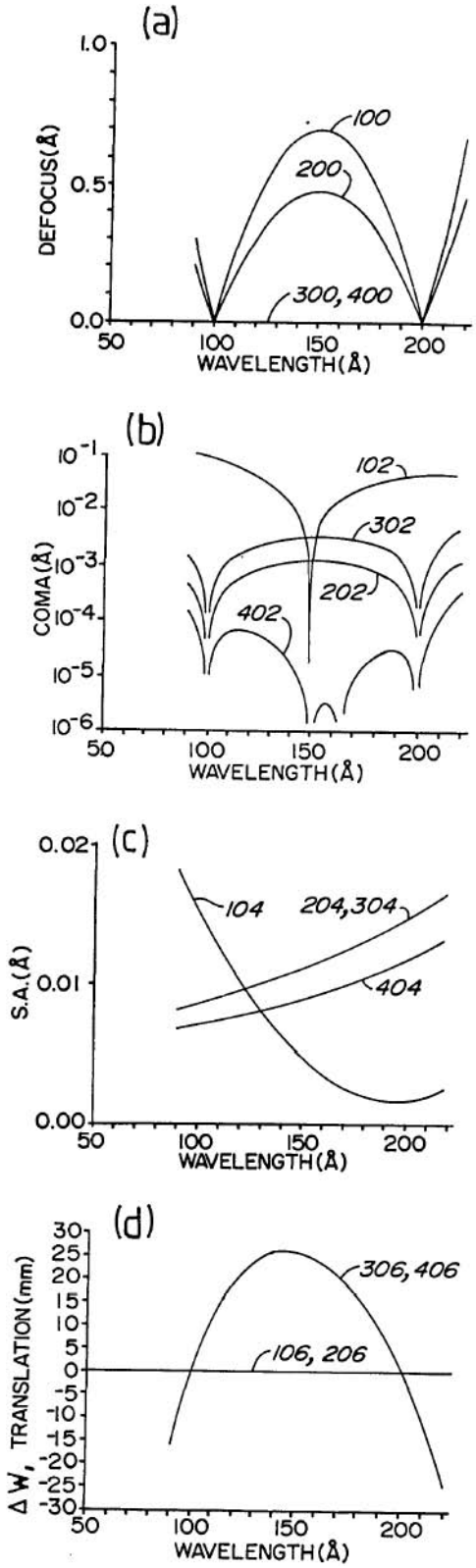


Fig. 2. Results of Fermat calculations using parameters for a grazing incidence monochromator: (a) first-order aberration of defocusing; (b) second-order aberration of coma; (c) third-order spherical aberration; and (d) grating surface translation. Curves 100–106 are for a classicial equally spaced spherical grating, which simply rotates about its pole to select the wavelength. Curves 400–406 are optimized for the new focusing condition, where a varied-space concave grating rotates about a fixed pole and translates along its ruled width. Given the same grating width, the new device exhibits a factor of 200 higher spectral resolution, limited only by spherical aberration. All aberrations are extrema (calculated from the edge of the grating aperture).

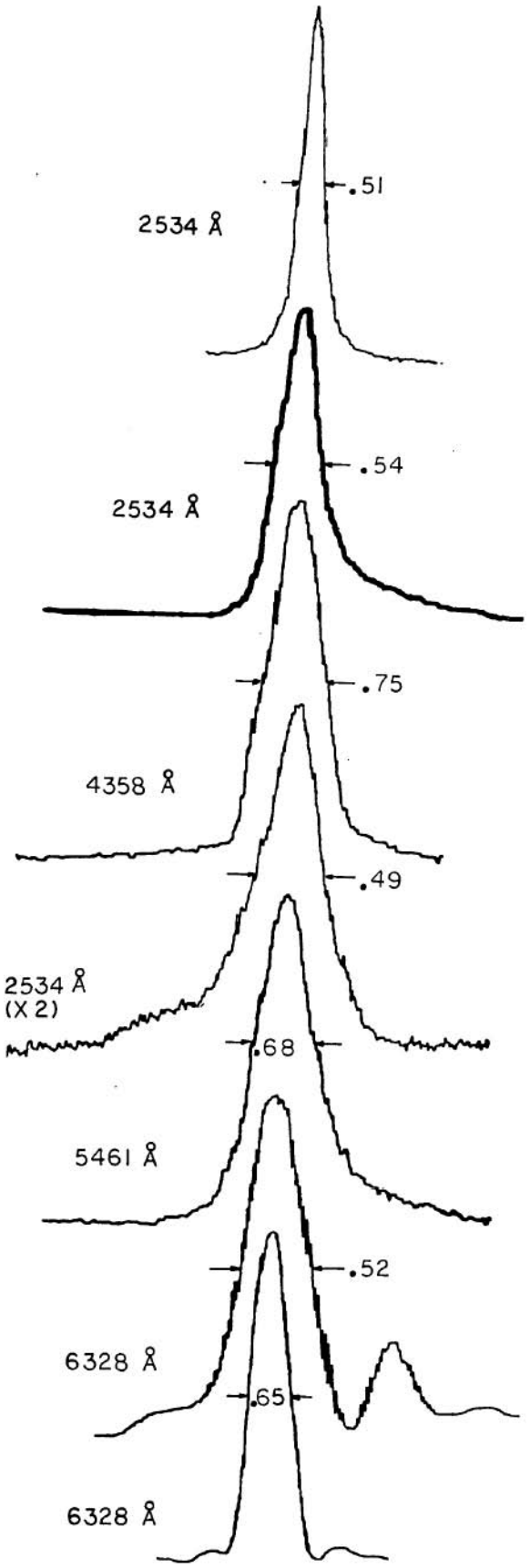


Fig. 3. Measured line profiles of a prototype in-focus monochromator, employing a single spherical grating reflection. Typical slit widths were 5–10 $\mu$m. These traces are not plotted on the same scale; however, the measured FWHM is indicated for each profile. The full grating aperture of 45 mm was used for all traces, except for the top and bottom traces where the aperture was stopped to ~36 mm to provide a centered illumination.

the ruled width coordinate $w = \Delta w$, and $w^*$ is measured relative to this new pole.

Using the same numerical parameters previously given and choosing $N_4 = 0$, curves 300, 302, and 304 of Fig. 2 result from numerically iterating Eqs. (14), (15), and (18) to eliminate defocusing at all wavelengths. All wavelengths are now sharply in focus, the new limit to the optical resolution being spherical aberration. As this term is proportional to the third power of the grating aperture, ~63% of the total diffracted energy is enclosed within an image width which is only one-fourth of the extreme aberration plotted in Fig. 2(c). The resulting spectral resolution is thus ~0.003 Å.

A further correction is available by use of nonzero values for $N_4$. From Eq. (16) it is clear that this term will significantly change the substituted value of $N_3^*$ as the grating is translated ($\Delta w \neq 0$). Curve 402 reveals the elimination of the coma at a third wavelength near the spectrum center by the choice of $N_4 = -6.99 \times 10^{-7}\ \mathrm{mm}^{-4}$. In practice the coma becomes negligible at all wavelengths, resulting in a highly symmetrical image whose remaining spherical aberration (curve 404) may be deconvolved from a spectrum by the use of accurate modeling techniques.

Because the grating radius and rotation provide for the broad selection of wavelength, the amount of space variation required is small and easily accomplished with present technology. As plotted in Fig. 2(d), the maximum amount of translation is only 25 mm. A 75-mm ruled grating width, with an aperture stop (Fig. 1) to constrain an exactly fixed beam direction, will provide the assumed 50-mm illuminated aperture. Alternatively, the full 75 mm may be utilized at all wavelengths if the incident beam overilluminates the grating and a ±15% deviation is allowed in the direction of the ray diffracted from the center of the aperture.

The small amount of translation also enables the use of a simple linear translation stage, the resulting vertical movement of the intersection point of the concave grating surface with the principal ray being unimportant. This maintains fixed directions for the incident and diffracted rays. Furthermore, because the grating translation functions only to remove a residual amount of defocusing, the required accuracy of translation is modest.

Experimental verification of the above new theory has been accomplished by construction of a breadboard developmental version of this monochromator. To demonstrate the grazing incidence performance and hence the applicability of this design to short wavelengths, the included angle ($\alpha + \beta$) of the principal ray was chosen to be 140° (20° graze at zero order). The numerical parameters were chosen to enable operation in the ultraviolet and visible regions of the spectrum so as to allow alignment and testing in atmosphere. The resulting groove density was 200 g/mm at the grating center, the radius of curvature of the spherical grating was 1001 mm, the object distance was 301.5 mm, image distance was 316.6 mm, and the full grating aperture was 45 mm. For this demonstration, the grating translation was provided by a manual micrometer and ball slide, and the rotation driven by a precision lead screw and wavelength bar. At each wavelength tested, the translation was experimentally adjusted to maximize the detected power. Then a high resolution scan across the spectral line was traced on a chart recorder. Two light sources were used: a low pressure mercury lamp and a He–Ne laser. The mercury discharge was ~5 mm in diameter and placed behind the entrance slit, whereas the collimated laser pencil beam ~0.6 mm in diameter was simply diffracted by the entrance slit to illuminate the full grating aperture.

Figure 3 shows the wavelength profiles obtained for three strong emission lines of the Hg lamp and the red line of the He–Ne laser. These traces reveal a symmetrical centrally peaked in-focus image at each wavelength. As listed in Table I, which includes an additional three (weaker) Hg lines, all measured resolutions are attributed entirely to either the finite slit widths or the physical diffraction-limited resolution (9000 grooves full aperture). In agreement with both geometrical (Fermat) calculations and numerical ray tracing of the line profiles, the obtained resolution of <1 Å is approximately a factor of 4 less than the extremum spherical aberration calculated to be 3–5 Å for wavelengths of 2534 to

**Table I. Predicted and Measured Monochromator Performance[a]**

| $m$ | λ(Å) | $\Delta w$(mm) Theory | $\Delta w$(mm) Actual | $\Delta\lambda_d$(Å) | $s_0$(μm) | $s_i$(μm) | $\Delta\lambda_0$(Å) | $\Delta\lambda_i$(Å) | Δλ(Å) Actual |
|---|---|---|---|---|---|---|---|---|---|
| Uncertainty (±) | | | 0.2 | | 1 | 1 | 0.08 | 0.05 | 0.05 |
| 1 | 2534 | 0.00 | 0.12 | 0.28 | 10 | 10 | 0.68 | 0.88 | 0.82 |
| 1 | 2534 | | | 0.28 | 10 | 5 | 0.68 | 0.22 | 0.73 |
| 1 | 2534 | | | 0.36[b] | 5 | 5 | 0.34 | 0.22 | 0.51 |
| 1 | 3126 | 6.10 | 6.30 | 0.35 | 20 | 20 | 1.41 | 0.81 | 1.35 |
| 1 | 3126 | | | 0.35 | 10 | 10 | 0.70 | 0.40 | 0.75 |
| 1 | 3650 | 8.39 | 8.37 | 0.41 | 20 | 20 | 1.46 | 0.76 | 1.35 |
| 1 | 4047 | 8.86 | 8.82 | 0.45 | 10 | 10 | 0.75 | 0.36 | 0.72 |
| 1 | 4358 | 8.88 | 8.67 | 0.48 | 10 | 10 | 0.76 | 0.35 | 0.75 |
| 2 | 2534 | 6.84 | 6.52 | 0.14 | 10 | 10 | 0.40 | 0.16 | 0.49 |
| 1 | 5461 | 5.14 | 4.97 | 0.61 | 10 | 10 | 0.81 | 0.30 | 0.68 |
| 1 | 5461 | | | 0.61 | 5 | 10 | 0.40 | 0.30 | 0.56 |
| 1 | 6328 | 0.00 | 0.00 | 0.70 | 10 | 5 | 0.85 | 0.13 | 0.64 |
| 1 | 6328 | | | 0.70 | 5 | 5 | 0.42 | 0.13 | 0.52 |
| 1 | 6328 | | | 0.87[b] | 10 | 5 | 0.85 | 0.13 | 0.65 |
| 1 | 6328 | | | 0.87[b] | 5 | 5 | 0.42 | 0.13 | 0.65 |

[a] $m$, spectral order; λ, wavelength; $\Delta w$ (theory), predicted grating translation; $\Delta w$ (actual), measured grating translation relative to 0-μm reading for optimized imaging at λ = 6328 Å; $\Delta\lambda_d$, diffraction-limited resolution, assuming a full grating aperture; $s_0$, entrance slit width; $s_i$, exit slit width; $\Delta\lambda_0$, entrance slit-limited resolution; $\Delta\lambda_i$, exit slit-limited resolution; Δλ (actual), measured FWHM of traced line profile.

[b] Grating width stopped to 36 mm, centered at the rotation axis.

6328 Å. A few of the profiles in Fig. 3 can be seen to have a slightly higher wing to one side of the peak. This is due to the grating translation (9 mm, as given in Table I), which weights the aperture and thus the spherical aberration to one side of the grating pole. This effect is removed by stopping this small fraction of the aperture, resulting in the symmetrical profiles shown in the top and bottom traces of Fig. 3. The diffraction-limited profile at 6328 Å is evidenced by the presence of subsidiary maxima.

The measured FWHM of these profiles, using slit widths of 5–10 $\mu$m, represents resolving powers $\lambda/\Delta\lambda$ = 5000–12,000 for this grazing incidence monochromator of only 0.6 m in length and a meridional aperture of 0.05 rad. A conventional spherical grating would exhibit a defocusing of 35 Å at the center of this spectral region ($\lambda/\Delta\lambda$ = 125).

The ability to maintain the spectral focus for large grating apertures provides higher throughput than previous designs,[3,9] making the in-focus monochromator (IFM) particularly advantageous when operated with soft x-ray radiation. When used with conventional laboratory sources (electron bombardment, spark gap, Penning, and hollow cathodes), a single element IFM as discussed above is appropriate. However, to maintain bright images when operating with low emittance sources, such as laser-produced plasmas and synchrotron radiation, stigmatic versions of the monochromator are required. This may be accomplished without degradation of spectral resolution by the insertion of a mirror which provides focusing in the direction normal to the grating dispersion. For example, a 1-m long stigmatic IFM having a geometrical collection aperature of $\sim 1 \times 10^{-3}$ sr would provide an optical resolving power of $10^3$ in the 35–500-Å wavelength region.

Commercial models of the IFM are being developed by Hettrick Scientific, Inc., which holds a license for manufacture, sale, and use of these devices. U.S. and foreign patents are pending on the general technique of combined rotation and translation of a varied-space grating, one embodiment of which has been described in this Communication.

The author thanks George Hirst for fabrication of the grating and loan of a detector used in the measurements reported here.

## References

1. H. A. Rowland, "On Concave Gratings for Optical Purposes," Philos. Mag. **16,** 197–210 (1883).
2. F. C. Brown, R. C. Bachrach, and N. Lien, "The SSRL Ultrahigh Vacuum Grazing Incidence Monochromator: Design Characteristics and Operating Experience," Nucl. Instrum. Methods **152,** 73–79 (1978).
3. M. C. Hettrick, "High Resolution Gratings for the Soft X-Ray," Nucl. Instrum. Methods **A266,** 404–413 (1988).
4. M. Itou, T. Harada, and T. Kita, "Soft X-Ray Monochromator with a Varied-Space Plane Grating for Synchrotron Radiation: Design and Evaluation," Appl. Opt. **28,** 146–152 (1989).
5. H. Dietrich and C. Kunz, "A Grazing Incidence Vacuum Ultraviolet Monochromator with Fixed Exit Slit," Rev. Sci. Instrum. **43,** 434–442 (1972).
6. W. R. Hunter, R. T. Williams, J. C. Rife, J. P. Kirkland, and M. N. Kabler, "A Grating/Crystal Monochromator for the Spectral Range 5 eV to 5 KeV," Nucl. Instrum. Methods **195,** 141–153 (1982).
7. H. Petersen, "The Plane Grating and Elliptical Mirror: A New Optical Configuration for Monochromators," Opt. Commun. **40,** 402–406 (1982).
8. T. Namioka, "Theory of the Concave Grating III. Seya-Namioka Monochromator," J. Opt. Soc. Am. **49,** 951–961 (1959).
9. M. C. Hettrick and J. H. Underwood, "Stigmatic High Throughput Monochromator for Soft X Rays," Appl. Opt. **25,** 4228–4231 (1986).
10. D. E. Aspnes, "High-Efficiency Concave-Grating Monochromator with Wavelength-Independent Focusing Characteristics," J. Opt. Soc. Am. **72,** 1056–1061 (1982).

## Double-headed Dragon monochromator for soft x-ray circular dichroism studies

Chien-Te Chen, Francesco Sette, and Neville V. Smith

AT&T Bell Laboratories, Murray Hill, New Jersey 07974.
Received 4 June 1990.
Sponsored by William R. Hunter, Springfield, Virginia
0003-6935/90/314535-02$02.00/0.


*Efficient differentiation between the left and right circular polarization of soft x-ray synchrotron radiation is achievable by doubling the number of prefocusing mirrors in a Dragon monochromator. The design also permits easy reversion to conventional linear polarization operation.*

An important property of synchrotron radiation from electron storage rings is the high degree of circular polarization just above or just below the plane of the ring.[1] In the vacuum ultraviolet (VUV) region, this property has been exploited in numerous spin-polarized photoemission studies.[2,3] In the x-ray region, the number of circular polarization studies is still relatively sparse.[4,5] To maximize the detection sensitivity, it is necessary to alternate between left and right circular polarization without affecting the position, energy resolution, or wavelength of the photon beam. In the VUV region ($h\omega \lesssim 30$ eV), where it is possible to work at normal incidence with large aperture gratings, this capability is readily achieved at the sample using masks and choppers.[6] In the hard x-ray region, an analogous approach can be employed because of the nongrazing incident angles of the photon beam on crystal monochromators and the small angular separation between beams of different polarization compared with the monochromator crystals' rocking curve.[4] These approaches are not immediately transferable to the soft x-ray region, where the need for grazing incidence optics requires prohibitively long gratings.

Our Dragon monochromator[7] at the National Synchrotron Light Source has recently been modified to perform circular dichroism studies without affecting its superior high resolution and flux performances.[5] The modifications, illustrated in Fig. 1, involve laborious coordinated translations of the entrance slit and a vertical focusing mirror as well as a recalibration of the wavelength scale. This precludes rapid alternation between left and right circular polarization and imposes limits on the sensitivity of the measurements.

Our solution to this problem is the double-headed (DH) Dragon. The basic idea, illustrated in Fig. 2, is to replace the horizontal focusing mirror (HFM) and vertical focusing mirror (VFM) at the head of the original Dragon with two identical pairs of mirrors $HFM_1$, $VFM_1$ and $HFM_2$, $VFM_2$. In the configuration of Fig. 2(b), $VFM_1$ ($VFM_2$) intercepts radiation below (above) the plane of the ring. Both VFMs focus onto the fixed entrance slit and illuminate the grating at the same angle, so that the wavelength calibration and resolution are the same for both beams. Each beam is delivered simultaneously to the sample region, and the position of the two beams is identical in the vertical plane, while it can be